Research Article

Yi Wang, Jun Wang*, Jie Wang, and David Hui

# Experimental and multiscale numerical investigations on low-velocity impact responses of syntactic foam composites reinforced with modified MWCNTs

https://doi.org/10.1515/ntrev-2021-0064
received July 13, 2021; accepted July 27, 2021

**Abstract:** This study focused on experimental and numerical investigations into the low-velocity impact behavior of epoxy resin matrix syntactic composites with embedded hollow glass microspheres (HGMs) and multiwalled carbon nanotubes (MWCNTs). The synergistic effects of HGMs and MWCNTs on the mechanical properties of epoxy resin composites were improved by applying amine and acid treatments to HGMs and MWCNTs, respectively. The influence of the MWCNT content and the applied impact energy on the impact responses and compression strength after the impact of these syntactic foam panel samples were discussed. The results indicated that modifying HGMs and MWCNTs contributed to improving the energy absorption and the strength retention factor (SRF) of these panels and the SRF increased with increased MWCNT content. Moreover, multiscale finite-element (FE) models were developed to simulate panel impact behavior, and modeling results were compared with experimental data. Then, the verified FE model was used to analyze the influence of CNT types (helical CNTs *vs* MWCNTs) and the diameter-to-thickness ratios of HGMs. This study provided a theoretical basis and design reference for a novel lightweight composite material subjected to low-velocity impact, which could be applied as a core material for sandwich structures in aerospace, marine engineering, transportation, and civil infrastructures.

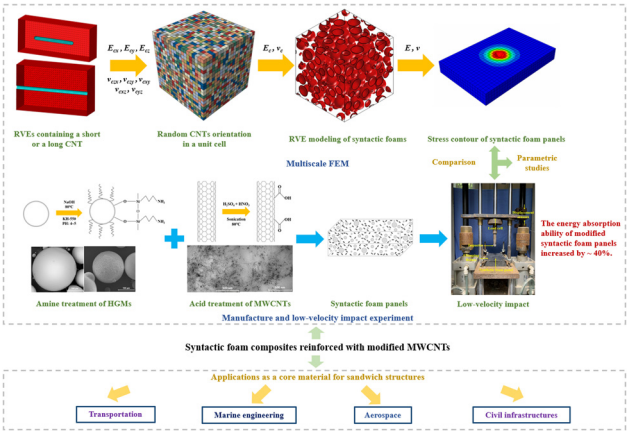


Graphical abstract

**Keywords:** syntactic foam, CNTs, low-velocity impact, CAI strength, multiscale FE model

## 1 Introduction

Syntactic foams consisting of hollow glass microspheres (HGMs) embedded in an epoxy matrix provide remarkable weight savings, high compressive strength, high energy absorption, and excellent buoyant behavior. They have experienced widespread applications in marine equipment, aerospace, and automotive components and as the core of sandwich structures [1–3]. Extensive studies have been performed evaluating the static [4–6], dynamic [7–9], and cyclic [10] behaviors of syntactic foams. Previous research has illustrated that the mechanical properties of syntactic foams can be tailored by altering their constituents. Although syntactic foams with a high volume fraction of microspheres can provide a weight-saving structure, some critical properties, such as compressive, tensile, and flexural properties and fracture toughness, are reduced due to the high crosslink density of the epoxy

* **Corresponding author: Jun Wang,** Bridge Engineering Department, College of Civil Engineering, Nanjing Tech University, Nanjing, 211816, China, e-mail: wangjun3312@njtech.edu.cn
**Yi Wang:** Structural Engineering Department, College of Civil Engineering, Nanjing Tech University, Nanjing, 211816, China
**Jie Wang:** RiseSun Real Estate Development Co., Ltd., Bengbu, 233000, China
**David Hui:** Department of Mechanical Engineering, University of New Orleans, New Orleans, LA 70148, United States of America

matrix, which limited their application [11]. Hence, developing syntactic foams with low density and superior mechanical properties is of great interest. In this study, a novel MWCNT-reinforced syntactic foam is developed, in which MWCNTs and microspheres were chemically modified to achieve high dispersion and improve interfacial adhesion in an epoxy matrix. The low-velocity impact responses of the modified syntactic foam panels are investigated to understand the energy absorption ability, CAI strength, and associated failure mechanisms. The resulting novel syntactic foam sandwich panels are expected to be lightweight, highly energy-dissipative, and corrosion-resistant enabled for potential applications in explosion vents, carriages, submarines, airframes, and anticollision guard rails and bumpers. The process is shown in the graphical abstract.

An effective strategy for improving the characteristics of syntactic foams is to promote interfacial adhesion between glass spheres and the polymer matrix by surface treatment. Zengin *et al.* [12] have reported that the surface properties of glass spheres can be improved by functionalization (modified first with 3-aminopropyltriethoxysilane and then treated with different polycarboxylic acid polymers and poly copolymers). Zhang *et al.* [13] have applied a hierarchical inorganic/organic hybrid surface modification strategy (HGMs modified by hierarchical NiCo-LDH nanosheets and DOPO-based silane coupling agent) to enhance interfacial adhesion between HGMs and the epoxy matrix. Fabricating amine-terminated HGMs is considered to be one of the best surface treatment technologies [14]. NaOH is a favorable agent for attaching hydroxyl groups on HGM surfaces for the subsequent reaction with a silane coupling agent in the fabrication of amine-terminated HGMs because it is much less toxic than hydrochloric and sulfuric acids [14,15].

Carbon nanotubes (CNTs) have been developed mainly to form tailorable properties for different engineering applications, providing outstanding mechanical properties and thermal stability. Insertion of CNTs is a promising approach for reinforcing syntactic foams without much variation in density [16,17]. The incorporation of a small content of CNTs into a resin matrix can improve load transfer effects, prevent crack propagation, and thus, enhance the overall mechanical performance [18,19]. Esmaeili *et al.* [20] have stated that the tensile strength and Young's modulus of epoxy composites are improved at 0.1 and 0.25 wt% MWCNTs. Further increasing the MWCNT content to 0.5 wt% has been found to lead to decreased tensile characteristics of epoxy composites due to inhomogeneous MWCNT dispersion [20]. Wang *et al.* [21] have reported that incorporating MWCNTs (1 wt%) and short Kevlar fibers (8.3 g/m$^2$) into the epoxy can enhance the shear strength of epoxy-bonded steel substrates by 70% due to a bridging and pullout-toughening mechanism. Laurenzi *et al.* [22] have reported that MWCNTs can significantly improve the ballistic properties of composite laminates under energies of 377 and 1,750 MJ, but exhibited poor response under higher energy of 4,202 MJ. High amounts of CNT additives tend to agglomerate in the resin matrix due to van der Waals forces, thus hindering full utilization of the superior properties of CNTs.

Functionalization of CNTs is a promising strategy for enhancing dispersibility and interfacial bonding between CNTs and epoxy matrix [23–26]. Li *et al.* [27] have reported that epoxy composites reinforced with 0.5 wt% MWCNT modified by acid treatment and triethylenetetramine (TETA) had 30% higher tensile strength and 34% higher impact strength than pure epoxy composites. Guzman *et al.* [28] have studied the mechanical properties of syntactic foams reinforced with carboxylic acid-functionalized CNTs through a dispersion process comprising ultrasonic, calendaring, and vacuum centrifugal mixing. They have reported that the compressive strength and lap shear strength of functionalized CNT-reinforced syntactic foams processed at high vacuum (0.2 kPa) is significantly enhanced compared with those of pristine syntactic foams and that the glass transition temperature increased to 22°C for composites processed at a high vacuum with 0.5 wt% functionalized CNTs [28]. Ya *et al.* [29] have investigated the performance of syntactic foams reinforced with carboxylic CNTs modified with three noncovalent functionalization surfactants (polyethylene glycol, chitosan, and polymethylphenyl siloxane). They found that hybrid functionalization can effectively cover the defects on carboxyl CNT surfaces and thus improve molecular structural integrity. Ciecierska *et al.* [30] have stated that CNTs modified with amino groups can be dispersed uniformly in the epoxy matrix, thereby increasing the matrix crosslinking density. Previous studies have demonstrated that chemical treatment cooperated with a properly mixed approach can effectively improve the dispersion of CNTs in resin matrices.

Syntactic foam displays excellent tensile and shear ductility at low strain rates and partially retains these properties at high strain rates, making it an appealing core material for impact-resistant sandwich constructions. Characterization of the impact properties of syntactic foams has provided useful information for the development of impact-resistant members and impact energy absorbers in the transportation industries and infrastructures. The impact responses of syntactic foam and CNT-polymer composites have been reported in the

literature. A study by Ghosh *et al.* [31] has indicated that the size of glass microspheres (20 *vs* 40 μm) had negligible effects on the quasistatic behavior of syntactic foams, while foams with smaller microspheres had much higher energy absorption capacity than foams with larger microspheres at high-strain rates (~$10^3$/s). Pham *et al.* [32] have stated that the impact energy absorption of syntactic foams increases significantly with density and wall thickness of the macrospheres (average diameter: 3.5 mm ). Ahmadi *et al.* [33] have studied high-velocity impact responses of nanoreinforced syntactic foam sandwich panels. They found the specific perforation energy of a panel with a 40% volume fraction of microspheres is higher than those of panels with 20 and 60% volume fraction and the ballistic limit velocity of nanoclay-reinforced syntactic foam cores increased up to 10%. Siegfried *et al.* [34] have studied the effects of CNTs on the impact damage resistance of carbon-fiber-reinforced polymer (CFRP) composites. They found that CNTs contribute to improving the mode II interlaminar fracture toughness and damage tolerance of CFRP, but yielded CFRP more susceptible to the onset of epoxy matrix cracks, leading to a larger delamination area after impact.

The authors have investigated the mechanical behaviors of syntactic foam with different contents of hollow glass microspheres and MWCNTs [35]. Increasing the microsphere content can effectively increase the energy absorption ability of syntactic foams, while the addition of MWCNTs has insignificant effects on the impact resistance and energy absorption ability of syntactic foam because of MWCNT agglomeration in the epoxy resin matrix. To fully utilize the superior properties of CNTs and syntactic foams, the present study was focused on the low-velocity impact responses of MWCNT-reinforced syntactic foams, in which MWCNTs and microspheres were chemically modified to achieve high dispersion and enhanced interfacial adhesion in an epoxy matrix. Microstructural characterization experiments of modified MWCNTs and microspheres were performed by infrared spectroscopy, scanning electron microscopy (SEM), and transmission electron microscopy (TEM). The influences of the MWCNT content and the applied impact energy were discussed in detail. Moreover, multiscale finite-element (FE) models were developed to simulate the impact behavior of syntactic foams and the numerical results were compared with the experimental data. Then, the verified FE model was used to analyze the influence of CNT type and HGM diameter-to-thickness ratios (D/T) on the impact responses of these panels.

# 2 Materials and experimental methods

## 2.1 Materials

Epoxy resin GE-7118A (Wells Advanced Materials Co., Ltd., Shanghai, China) with the compatible hardener GE-7114B at a 10/3 weight ratio was used as the binder. Their properties as provided by the manufacturer were as follows: density of 1,200 kg/$m^3$, compressive strength of 45 MPa, Young's modulus of 0.435 GPa, a flexural strength of 105 MPa, a flexural modulus of 2.91 GPa, a tensile strength of 68 MPa, a tensile modulus of 3.05 GPa, and Poisson's ratio of 0.33.

Hollow glass microspheres (HGM, K25; 3M Co., St. Paul, MN, USA) were applied as the filler material. The stated dimensions of these microspheres were from 25 to 95 μm, with a mean diameter of 55 μm. The HGMs have a thickness of 0.95 μm, a density of 0.25 g/$cm^3$, a compressive strength of 5.2 MPa, Young's modulus of 1.55 GPa, and Poisson's ratio of 0.21.

MWCNTs were obtained from Shengzhen Tuling Evolution Technology Co., Ltd. (Shengzhen, China) and used as reinforcements. Properties provided by the manufacturer were as follows: MWCNTs have outer diameters of 3–15 nm, length of 15–30 μm, purity of 97 wt%, bulk density of 2.1 g/$cm^3$, Young's modulus of 900 GPa, and Poisson's ratio of 0.19.

## 2.2 Modifications of HGMs and MWCNTs

### 2.2.1 Amine treatment procedure

NaOH solution was used for surface treatment of HGMs because it was less toxic than hydrochloric and sulfuric acids. HGMs were first dispersed in deionized water. After 2 h, the supernatant was filtered to remove broken microspheres and the remaining HGMs were then dried at 120°C for 1.5 h, thus removing deposits on HGM surfaces. The freshly dried HGMs were next added to a NaOH solution (0.3 M) and stirred at 80°C for 1.5 h to produce surface hydroxyl groups. The resulting HGM-OH was washed using distilled water until the pH reached 7 and then dried at 120°C for 1.5 h. About 10 g of pretreated HGMs was reacted with 1 g of 3-aminopropyl-triethoxysilane in a solution of ethanol/water (3/1, v/v, absolute EtOH/water), with the pH adjusted to 4–5 with acetic acid.

After refluxing the mixture at 55°C for 30 min and sonication at 60°C for 30 min, the resulting HGMs were collected by filtration and dried at 90°C for 1.5 h. The ethoxy groups of the silane coupling agent react with hydroxyl groups on the surface of HGMs to generate the HGM-$NH_2$ structure. The resulting density of these modified HGMs was 0.12 g/cm$^3$.

### 2.2.2 Acid treatment procedure

MWCNTs were added to an aqua regia solution of concentrated sulfuric and nitric acids at 3/1 (v/v) at room temperature to fabricate carboxylic functionalized MWCNTs. The mixed suspension was refluxed, condensed, and sonicated at a constant cycle (40 kHz and 200 W/cm$^2$) for 6 h in a three-neck flask. Prolonging the acid treatment time can create defects in the side walls of MWCNTs. Then, the suspension was diluted in deionized water and collected by filtration. The resulting carboxy acid MWCNTs were washed with deionized water and acetone until the pH reached ~7, and then dried in a vacuum oven at 110°C for 3 h. The density of the resulting modified MWCNTs is 1.98 g/cm$^3$.

## 2.3 Test specimens

First, epoxy resin was heated in an oil bath at 75°C to achieve the desired consistency, and then a hardener was added to the resin. Subsequently, the functionalized MWCNTs were mixed with the resin and the mixture was sonicated at 40 kHz for 30 min. This step can help to form strong hydrogen bonding between MWCNTs and the epoxy resin matrix. Then, the amine-treated HGMs were added to the mixture and stirred at 55°C in an oil bath for 30 min. Finally, the mixture was poured into a stainless-steel mold and cooled at room temperature for 24 h. The synthesis and preparation methods are shown in Figure 1.

Previous investigation [35] has indicated that the energy absorption ability of the syntactic foam with 70 vol% HGMs is higher than that of the syntactic foam with 50 vol%. Hence, the volume fraction of glass spheres in the matrix was set at 70% in this study. MWCNTs were added at 0.6 and 1.2 wt% in the matrix.

Compression testing was performed according to ASTM D1621-10 [36] with samples of dimension 100 mm$^3$ × 100 mm$^3$ × 50 mm$^3$, and tensile testing was performed according to ASTM D638-02a [37] with 165 mm$^3$ × 19 mm$^3$ × 5 mm$^3$ samples. Five equal coupons were tested for each material composition. Details of the test specimens for compressive and tensile tests are shown in Table 1.

Low-velocity impact testing was performed according to ASTM D7136M-15 [38] with 100 mm$^3$ × 150 mm$^3$ × 20 mm$^3$ panel samples. According to ref. [35], the energy absorption of syntactic foams with a sphere volume fraction of 70% was higher than that of foams with a sphere volume fraction of 50%. Hence, the sphere volume fraction of the specimens herein was determined as 70%. A total of 15 specimen groups were designed to investigate the influences of the surface treatment of HGMs, the content of modified and unmodified MWCNTs, and the applied impact energy on the dynamic response of syntactic foam panels. Three equal panel coupons were prepared and tested for each material composition and the applied impact energy. The peak-impact force and duration of each specimen were taken as the mean values of those of the three coupons. Details of test specimens for the low-velocity impact test are shown in Table 2. Moreover, compression after impact (CAI) testing was performed on specimens with impact damage according to ASTM D7137/7137M-12 [39]. Undamaged specimens were also tested to evaluate the influence of impact damage.

## 2.4 Experimental setup

Fourier transform-infrared spectroscopy (FT-IR; Nicolet iS50, Nicolet Instrument Corp., Madison, WI, USA) was

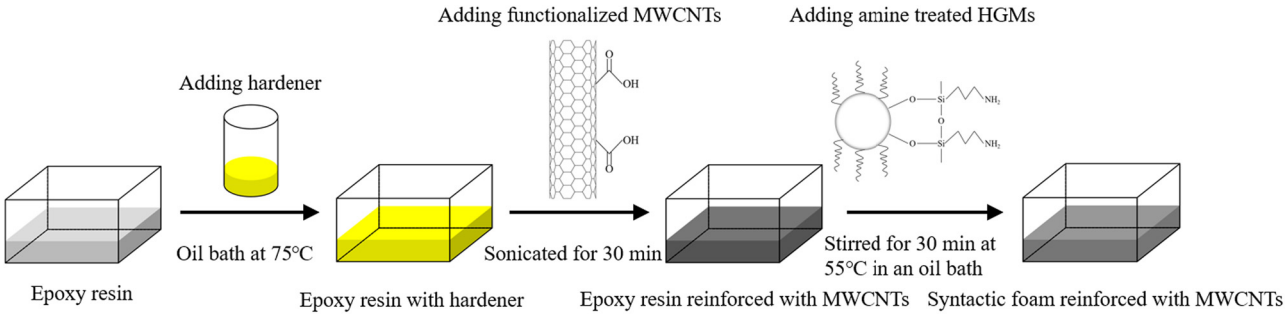


**Figure 1:** Synthetic and preparation method.

**Table 1:** Static properties of syntactic foam composites

| Specimens | Compressive strength (MPa)/$\delta$ (%) | Compressive modulus (GPa)/$\delta$ (%) | Tensile strength (MPa)/$\delta$ (%) | Young's modulus (GPa)/$\delta$ (%) | Density (kg/m$^3$) |
|---|---|---|---|---|---|
| F70 [35] | 18.39/3.73 | 0.60/2.35 | 7.81/4.31 | 0.66/4.00 | 535 |
| F70C0.6 [35] | 21.89/2.88 | 0.63/3.16 | 9.08/4.37 | 0.66/2.30 | 517 |
| F70C1.2 [35] | 23.49/3.78 | 0.71/1.92 | 9.31/5.74 | 0.74/5.77 | 501 |
| F70M | 30.33/3.25 | 0.73/5.47 | 14.10/4.53 | 0.91/7.68 | 430 |
| F70C0.6M | 25.40/1.08 | 0.68/4.25 | 9.27/2.63 | 0.72/10.56 | 537 |
| F70C1.2M | 32.47/2.54 | 0.78/4.01 | 9.80/3.68 | 0.76/9.45 | 540 |
| F70MC0.6M | 34.45/5.22 | 0.97/3.78 | 16.64/2.31 | 0.92/6.45 | 432 |
| F70MC1.2M | 36.01/3.87 | 1.06/2.96 | 17.85/6.56 | 0.96/8.23 | 434 |

Note: In the first row, 70 represent 70% volume fractions of the glass spheres, C represents the CNT-reinforced foam composites, and 0.6 and 1.2 represent the 0.6% and 1.2% CNT weight fractions respectively; $\delta$ is the coefficient.

**Table 2:** Summary of the impact test matrix

| Specimens | $m$ (g) | $T$ (ms) | $F_{max}$ (kN) | MPD (mm) | $E$ (J) | SEA (J/g) |
|---|---|---|---|---|---|---|
| F70-II [35] | 160.5 | 3.23 | 8.9 | 9.782 | 42.2 | 0.26 |
| F70C0.6-II [35] | 155.1 | 3.38 | 9.5 | 10.189 | 43.4 | 0.28 |
| F70C1.2-II [35] | 150.3 | 3.54 | 10.2 | 10.762 | 45.1 | 0.30 |
| F70M-I | 129.0 | 2.56 | 10.04 | 7.53 | 36.80 | 0.285 |
| F70M-II | — | 2.72 | 10.80 | 7.98 | 42.98 | 0.333 |
| F70M-III | — | 2.89 | 11.43 | 8.89 | 48.56 | 0.376 |
| F70C0.6M-I | 161.2 | 2.98 | 9.10 | 8.10 | 37.94 | 0.235 |
| F70C0.6M-II | — | 3.20 | 9.51 | 8.68 | 44.30 | 0.275 |
| F70C0.6M-III | — | 3.43 | 9.90 | 9.50 | 50.01 | 0.310 |
| F70C1.2M-I | 161.9 | 3.01 | 9.62 | 8.35 | 39.98 | 0.247 |
| F70C1.2M-II | — | 3.31 | 10.30 | 8.72 | 46.05 | 0.284 |
| F70C1.2M-III | — | 3.69 | 10.49 | 9.56 | 52.16 | 0.322 |
| F70MC0.6M-I | 129.6 | 2.82 | 11.02 | 7.80 | 39.56 | 0.305 |
| F70MC0.6M-II | — | 2.85 | 11.36 | 8.17 | 45.31 | 0.350 |
| F70MC0.6M-III | — | 3.02 | 12.05 | 9.28 | 50.43 | 0.389 |
| F70MC1.2M-I | 130.2 | 2.90 | 11.28 | 7.89 | 40.90 | 0.314 |
| F70MC1.2M-II | — | 2.92 | 11.50 | 8.20 | 47.01 | 0.361 |
| F70MC1.2M-III | — | 3.11 | 12.31 | 9.32 | 53.03 | 0.407 |

Note: I, II, and III represent applied impact energies of 43, 49, and 54 J, respectively.

employed to record the wave numbers of MWCNTs and microspheres from 15 to 27,000/cm. The microstructure MWCNTs and their distribution in epoxy matrices were investigated by TEM (Tecnai G2 F30 S-Twin, FEI Co., Hillsboro, OR, USA) at 300 kV. The microstructure of microspheres before and after amine treatment and in composite samples after impact were examined using a SU8010 SEM (Hitachi Instruments, Inc., Tokyo, Japan).

Comprehensive and tensile properties of the specimens were measured in a 600 kN universal testing machine at a load rate of 2 mm/min and the strain was recorded by strain rosettes with gauge lengths of 10 mm.

The low-velocity properties of the foam panels were evaluated using a drop-weight machine (Figure 2), with the impactor with a semicircular nose of diameter 16 mm and a drop hammer of 5.5 kg in mass. Three different drop heights were applied (0.8, 0.9, and 1.0 m), which corresponded to applied impact energies of 43–54 J. Each specimen was impacted only once. The four corners of a sample panel were clamped to avoid slippage and rotation. A piezoelectric sensor mounted onto the drop hammer was used to record the impact force histories and a micrometer gauge with a resolution of 0.01 mm was used to measure the maximal penetration depth (MPD) just after impact.

The CAI strength of these foam panel samples was evaluated by edgewise compressive tests on a universal testing machine with a capacity of 600 kN and a load rate of 1.25 mm/min (Figure 3). The compressive load was recorded by a load cell mounted on the top steel panel

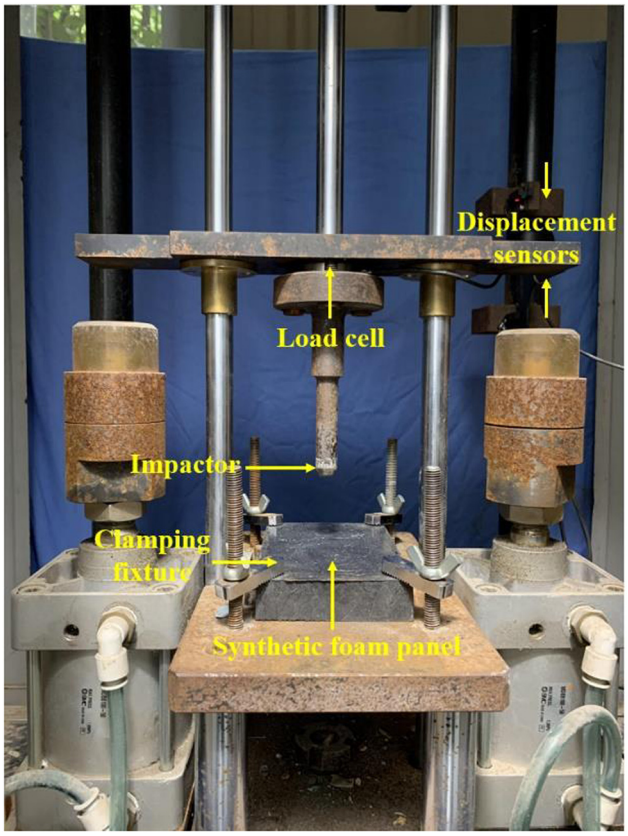


**Figure 2:** Test setup of drop-weight impact.

of the machine and the displacement was recorded automatically by the actuator. To minimize the stress concentrations of specimens at contact with loading panels and to ensure uniform load transfer, steel fixture systems were installed on both ends of the columns. All edgewise compressive testing specimens were loaded to reach a maximum load and load application continued until the residual load was reduced to 30% of its maximum load value.

# 3 Results and discussion

## 3.1 Structure and morphology of HGMs and MWCNTs

The FT-IR spectrum of amine-treated HGMs is shown in Figure 4a. The peak at 1,069/cm from modified HGMs corresponded to Si–O–Si bonds and stretching peaks at 1,630 and 3,440/cm to $NH_2$ groups. HGM morphologies before and after surface modification were examined by SEM and it was observed that pristine HGMs had smooth clean surfaces, while modified surfaces showed a dense layer due to reactions between –OH and 3-aminopropyltriethoxysilane (Figure 4b and c). FT-IR spectra and SEM confirmed that amine-treated HGMs had been successfully formed.

FT-IR spectra of MWCNTs were measured to characterize the acid treatment modification effects (Figure 5a). In modified MWCNTs, the peak at 1,631/cm was a typical carboxylic group stretching vibration (–COOH) and the peak at 3,440/cm related to –COO– stretching vibrations [27].

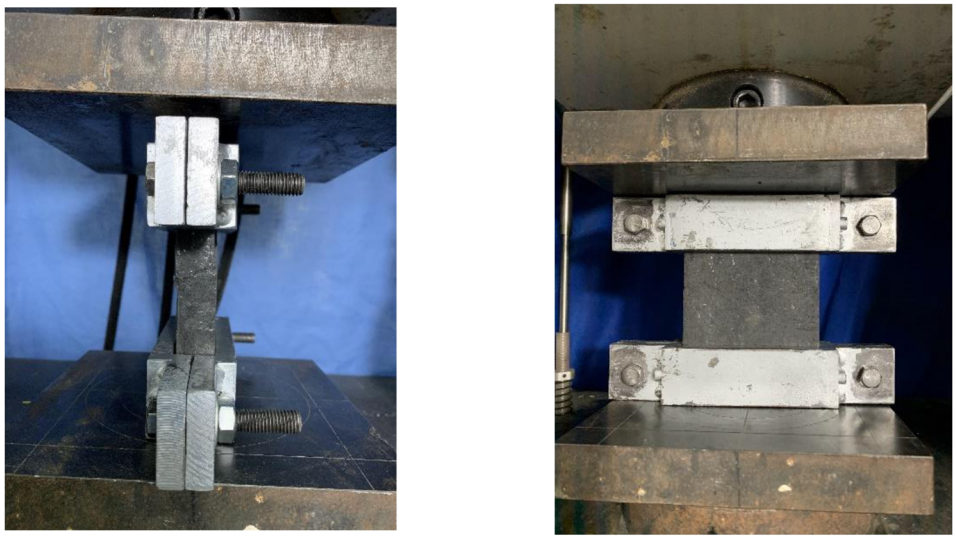

(a) (b)

**Figure 3:** Test setup of edgewise compression: (a) side view and (b) front view.

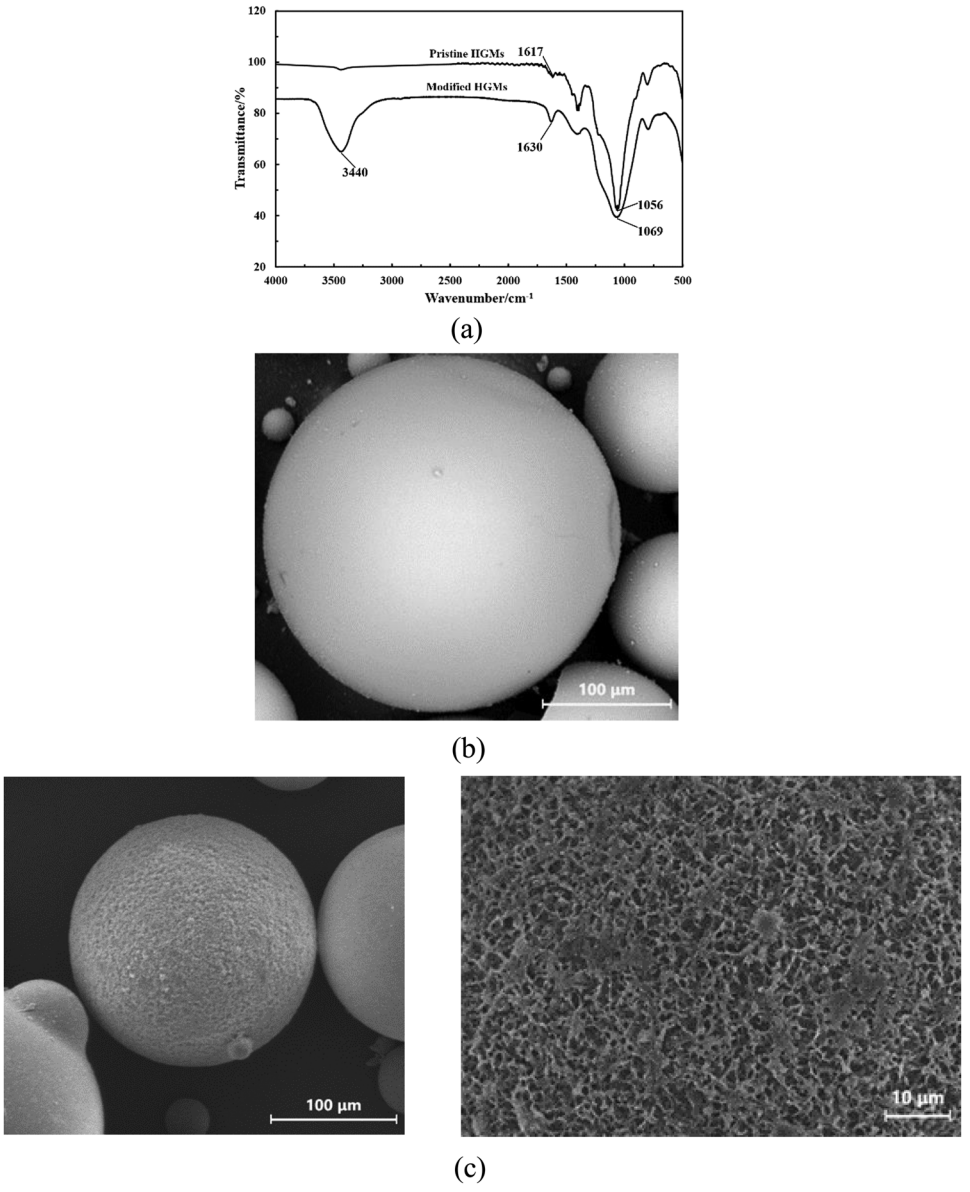


**Figure 4:** FTIP spectroscopy and SEM images of HGMs: (a) FTIP spectra of HGMs, (b) SEM image of unmodified HGMs, and (c) SEM images of modified HGMs.

Observation of the dispersion of MWCNTs in the epoxy matrix by TEM showed that unmodified MWCNTs were thin and vermicular accompanied by scattered agglomerations in the matrix (Figure 5b), while the average agglomerate size reduced after the addition of COOH-functionalized MWCNTs (Figure 5c).

## 3.2 Static properties

The compressive and tensile properties of the modified syntactic foam composite samples are listed in Table 1 and compared with those of unmodified samples. Compared with an unmodified syntactic foam composite (F70), the compressive strength and modulus of specimens with modified HGMs (F70M) were improved by 65 and 22%, respectively, and the tensile strength and modulus of specimens with modified HGMs (F70M) were improved by 81 and 38%, respectively. Compared with those of specimens with unmodified MWCNTs (F70C0.6 and F70C1.2), the compressive strengths of samples with 0.6 and 1.2 wt% modified MWCNTs (F70C0.6M and F70C1.2M) were improved by 38 and 48%, respectively. However, merely modifying MWCNTs had an insignificant influence on the compressive

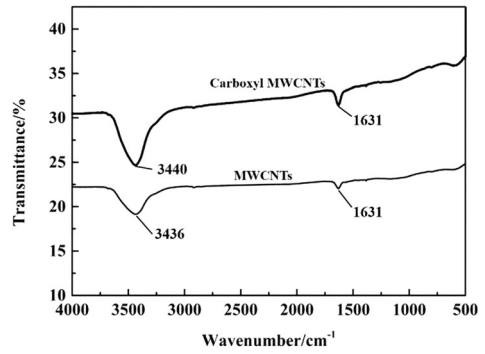


(a)

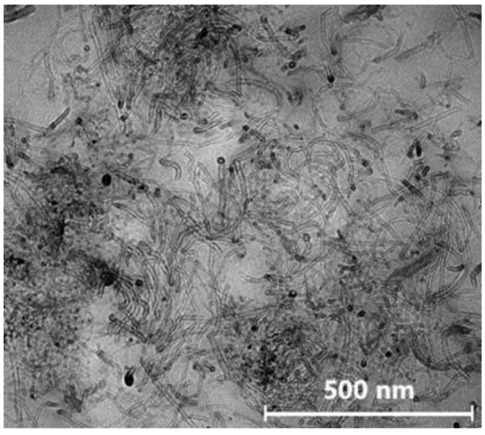


(b)

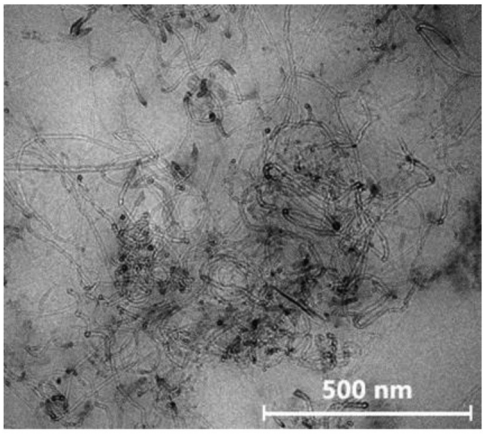


(c)

**Figure 5:** FTIP spectroscopy and TEM images of MWCNTs: (a) FTIP spectra of MWCNTs, (b) TEM image of unmodified MWCNTs in the epoxy matrix [35], and (c) TEM image of modified MWCNTs in the epoxy matrix.

modulus and tensile properties of these specimens. For specimens with modified HGMs and 0.6 wt% MWCNTs (F70MC0.6M), their compressive strength and modulus were improved by 57 and 54%, and tensile strength and modulus were improved by 83 and 39%, respectively, compared with the unmodified counterpart (F70C0.6). For specimens with modified HGMs and 1.2 wt% MWCNTs (F70MC1.2M), their compressive strength and modulus were improved by 65 and 68%, and tensile strength and modulus were improved by 97 and 46%, respectively, compared with the unmodified counterpart (F70C1.2). These results indicated that modifying HGMs by amine treatment had a more significant effect on improving the compressive and tensile properties of these foams than modifying MWCNTs by acid treatment.

## 3.3 Impact responses

All specimens had a circular dent in the center of the foam panel samples after impact (Figure 6). The MPDs of all specimens increased with increased applied impact energy. For example, increasing the applied impact energy from 43 to 49 and 54 J led to 4 and 18% increases, respectively, in the MPD for samples with modified HGMs and 1.2 wt% modified MWCNTs. Under the same applied impact energy of 49 J, the MPD of specimens with modified HGMs (F70M) was 18% shorter than that of unmodified specimens (F70). The MPD of specimens with modified MWCNTs (F70C0.6M and F70C1.2M) were 11% shorter than those of unmodified specimens (F70) and 15–19% shorter than those of specimens with unmodified MWCNTs (F70C0.6 and F70C1.2). Moreover, the MPD of specimens with modified HGMs and MWCNTs (F70MC0.6M and F70MC1.2M) were 20–24% shorter than those of specimens with unmodified HGMs and MWCNTs (F70C0.6 and F70C1.2). These results indicated that modifying HGMs by amine treatment and modifying MWCNTs by acid treatment both contributed to enhance the local stiffness of these foam samples.

The impact force history curves of sample panels exhibited similar half-sinusoidal profiles (Figure 7). Under the same applied impact energy of 49 J, specimens with modified HGMs (F70M) exhibited a 21% higher peak-impact force and 16% shorter duration than unmodified specimens (F70). Specimens with modified HGMs and modified MWCNTs had 13–20% higher peak-impact force and ~16% shorter duration than their unmodified counterparts (*i.e.*, F70MC0.6M-II *vs* F70C0.6-II). The rough surface of modified HGMs contributed to improving interfacial adhesion between the HGMs and resin matrix, and enhancing the impact resistance of HGMs. Under the same impact load, more unmodified HGMs were crushed than modified HGMs (Figure 8), as the resin mixed with more debris of crushed spheres thus had higher local stiffness and resulted in prolonged duration in specimens with unmodified HGMs. Merely modifying MWCNTs had an

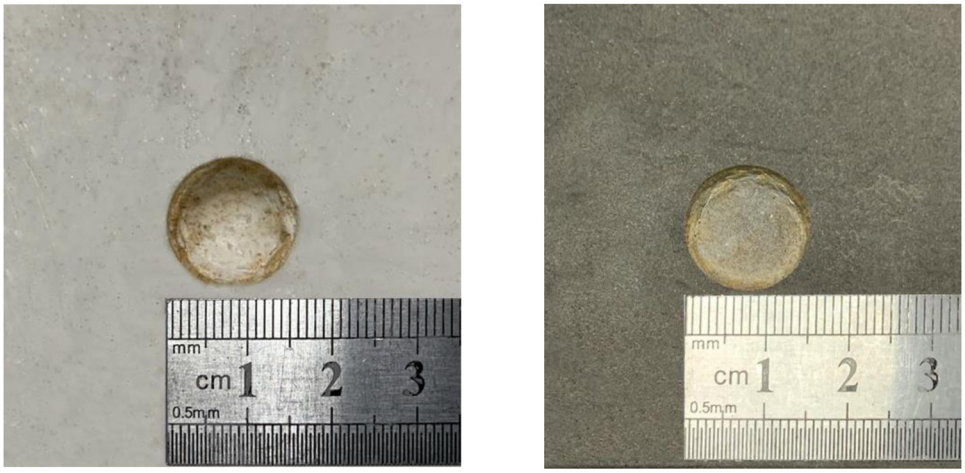


**Figure 6:** Impact damage of typical syntactic foam panels: (a) F70-III and (b) F70MC1.2M-III.

insignificant influence on the peak-impact force and led to only a little decrease in duration (*i.e.* F70C1.2-II *vs* F70C1.2M-II). This may be attributed to the low content of MWCNTs in syntactic foam panels. For specimens reinforced with modified MWCNTs, the peak-impact force was enhanced with an increased MWCNT content. Compared with those of unmodified specimens (F70), the highest increase in the peak-impact forces was 16% for specimens with unmodified HGMs and 1.2 wt% modified MWCNTs, and 29% for specimens with modified HGMs and 1.2 wt% modified MWCNTs at 43 J, respectively. These results indicated that modifying HGMs by amine treatment had more significant effects on enhancing the impact resistance of these samples than modifying MWCNTs by acid treatment. Moreover, increasing the applied impact energy from 43 to 54 J led to a slight increase (<10%) in the peak-impact force and duration.

The energy absorption $E$ can be obtained using the following classic relation:

$$E = \int_0^{\delta_{st}} F \, \mathrm{d}\delta, \tag{1}$$

where $F$ is the applied impact force and $\delta$ the corresponding vertical displacement.

The energy absorption parameters were calculated based on the recorded impact-displacement curves (Figure 9) and are listed in Table 2, in which SEA (specific energy absorption) is the energy absorption per unit mass.

Under the same applied impact energy of 49 J, the $E$ of specimens with modified HGMs (F70M) was almost identical to that of specimens with unmodified HGMs (F70), while the SEA of F70M was 28% higher than that of F70 because modified HGMs were much lighter than the unmodified HGMs. Meanwhile, compared with unmodified counterparts (*i.e.*, F70C1.2-II), the $E$ of specimens with modified HGMs and MWCNTs (*i.e.*, F70MC1.2M-II) increased insignificantly, while the SEA of the latter increased by ~25%. This is because amine treatment can not only improve the interface adhesion between HGMs and resin matrix but also decrease the density of syntactic foams. Merely modifying MWCNTs had an insignificant influence on $E$ and SEA (*i.e.*, F70C1.2-II *vs* F70C1.2M-II). For specimens reinforced with modified MWCNTs, the $E$ and SEA were enhanced slightly with an increased MWCNT content. Compared with those of unmodified specimens (F70), the highest increases in $E$ and SEA were 11 and 39% for specimens with modified HGMs and 1.2 wt% modified MWCNTs at 49 J, respectively. The cost of syntactic foams with modified HGMs and 1.2 wt% modified MWCNTs was ~10% higher than that of unmodified syntactic foams, indicating that the energy absorption ability of syntactic foams can be economically improved by incorporating modified HGMs and MWCNTs. Moreover, the SEA of F70MC1.2M-III was 46% higher than that of polyurethane foam composites in ref. [40], and almost the same as that of aluminum syntactic foam composites under the same applied impact energy [41]. In general, both modified HGMs and MWCNTs contributed to improving the energy absorption of these samples and the former had more significant effects in improving SEA than the latter because amine treatment decreased the HGM weight.

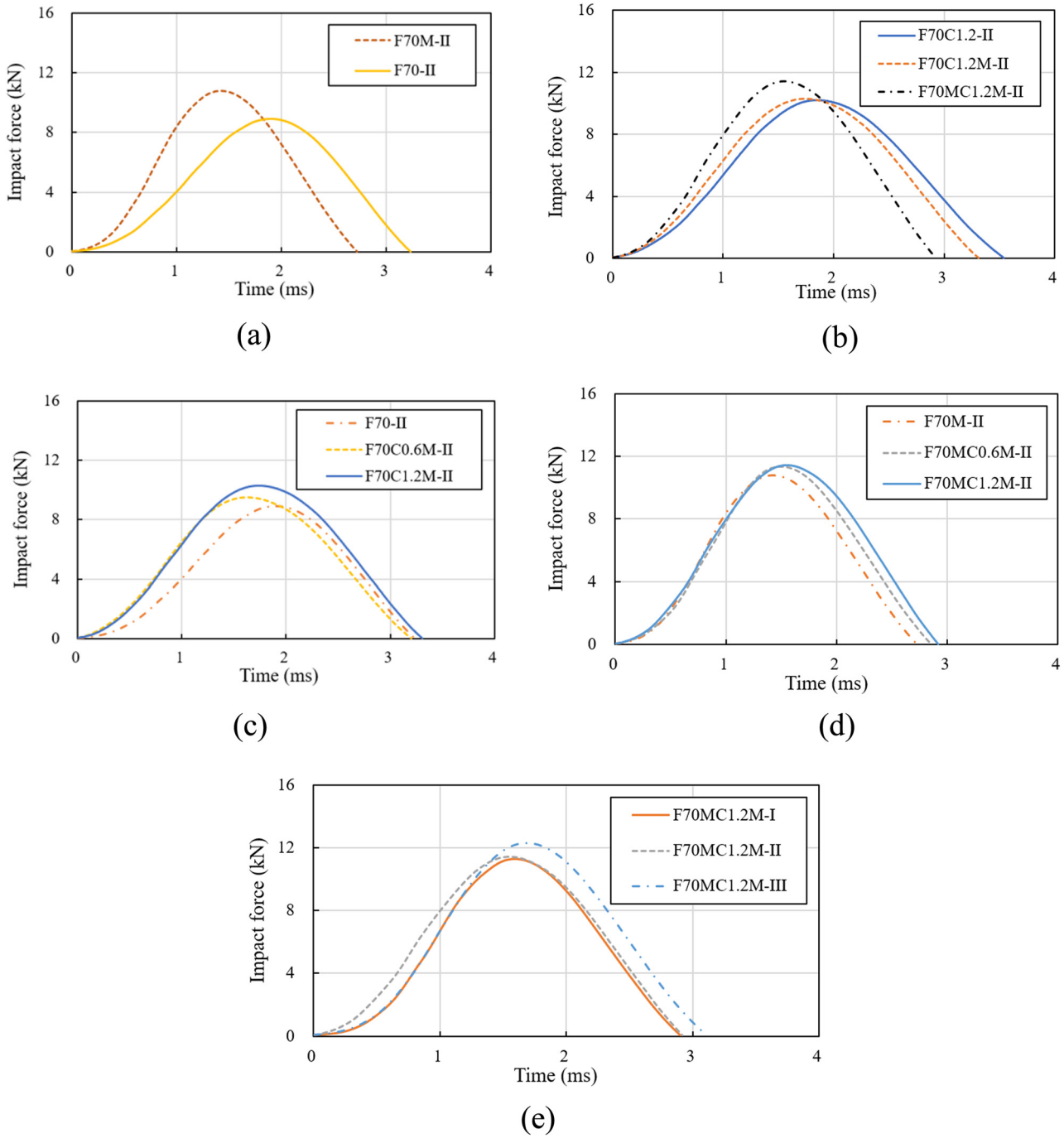


**Figure 7:** Impact force histories: (a) influence of the modified HGMs, (b) influence of the modified HGMs and MWCNTs, (c) influence of the contents of modified MWCNTs on specimens with unmodified HGMs, (d) influence of the contents of modified MWCNTs on specimens with modified HGMs, and (e) influence of the applied impact energy.

## 3.4 Edgewise compressive responses

Examination of the condition of typical specimens after edgewise compression showed that cracks of specimens without impact damage were initiated at the margin and then propagated to the opposite side, while the cracks of specimens with impact damage were initiated at the dent and then propagated to the margin (Figure 10). Only vertical or transverse cracks occurred in specimens without MWCNT reinforcements, while vertical, transverse, and diagonal cracks occurred in specimens reinforced with MWCNTs. This was because when the crack

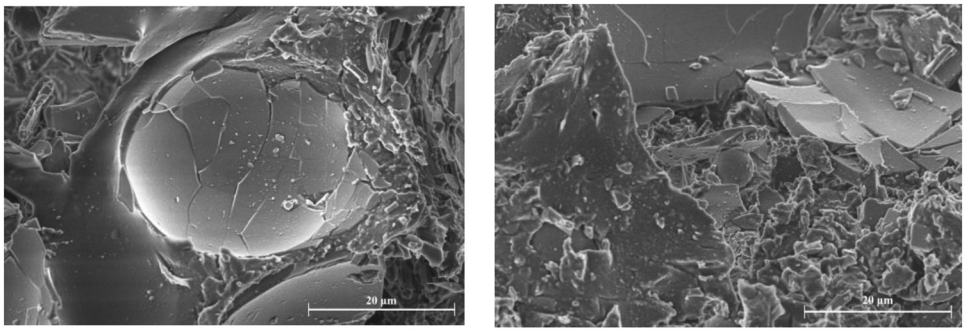


**Figure 8:** SEM of syntactic foam panels after impact: (a) F70MC0.6M-II and (b) F70C0.6-II.

tip encountered MWCNTs, the external force perpendicular to them caused MWCNTs to pull out of the epoxy resin or break, leading to changes in the crack propagation path.

To calibrate the comparison of edgewise compressive strength between intact specimens and specimens with impact damage, the strength retention factor (SRF) was defined as the ratio of the edgewise compressive capacity of specimens with impact damage to that of specimens without impact damage. The SRF of specimens with modified HGMs was higher than that of specimens with unmodified HGMs (F70 *vs* F70M, Table 3). In the case of the same applied impact energy and MWCNT content, the SRFs of specimens with modified MWCNTs were higher than those of specimens with unmodified MWCNTs and the SRFs of specimens with modified HGMs and MWCNTs were higher than those of specimens with unmodified HGMs and MWCNTs. Moreover, SRFs increased with increased MWCNT contents. This was attributed to the fact that modifying HGMs and MWCNTs enhanced the interfacial adhesion between filler-resin interfaces and MWCNTs prevented crack growth.

# 4 Finite-element modeling

Multiscale finite-element (FE) models were developed to simulate the impact behavior of these syntactic foam panel samples. First, a three-dimensional (3-D) nanoscale representative volume element (RVE) containing a single CNT was modeled to extract the equivalent mechanical properties of nano-heterostructures. Then, considering random CNT orientation and length, a 3-D microscale unit cell was modeled to predict the compressive properties of CNT-reinforced epoxy resin matrix composites. These compressive properties of CNT-epoxy composites were input as the mechanical parameters of the matrix of a 3-D macro-mechanical model consisting of 70-vol% HGMs randomly dispersed. Finally, the impact responses of sample panels reinforced by CNTs were analyzed in ABAQUS, in which the mechanical properties of the syntactic foams were extracted from the results of the macro-mechanical model.

## 4.1 RVEs of CNT-reinforced epoxy matrix

Square nanoscale RVEs containing a long or a short CNT were established to obtain uniaxial compressive, lateral contractive, and axial torsion properties. In each RVE, only one short or long CNT was aligned along the length direction of RVE. The CNT and matrix were assumed as continuous, linear elastic, isotropic, and homogeneous materials with specific Young's moduli, and the CNT bonded perfectly with the matrix [42–44]. Therefore, the effective material constants of RVEs, *i.e.*, Young's moduli $E_{cx}$ (=$E_{cy}$), $E_{cz}$, and Poisson's ratios $\nu_{cxy}$ and $\nu_{czx}$ (=$\nu_{czy}$) were determined by uniaxial tensile, lateral contractive, and axial torsion tests on RVEs (Figure 11 [45,46]):

$$E_{cz} = \frac{\sigma_{cz}}{\varepsilon_{cz}} = \frac{L}{\Delta L}\bar{\sigma}_{cz}, \tag{2}$$

$$\nu_{czx} = \left(\frac{\Delta a}{a}\right)\Big/\left(\frac{\Delta L}{L}\right), \tag{3}$$

$$E_{cx} = E_{cy} = \frac{2}{\frac{1}{2G_{cxy}} + \frac{2\nu_{czx}^2}{E_{cz}} + \frac{\Delta x}{pa}}, \tag{4}$$

$$\nu_{cxy} = \frac{1}{G_{cxy}\left(\frac{1}{2G_{cxy}} + \frac{2\nu_{czx}^2}{E_{cz}} + \frac{\Delta x}{pa}\right)} - 1, \tag{5}$$

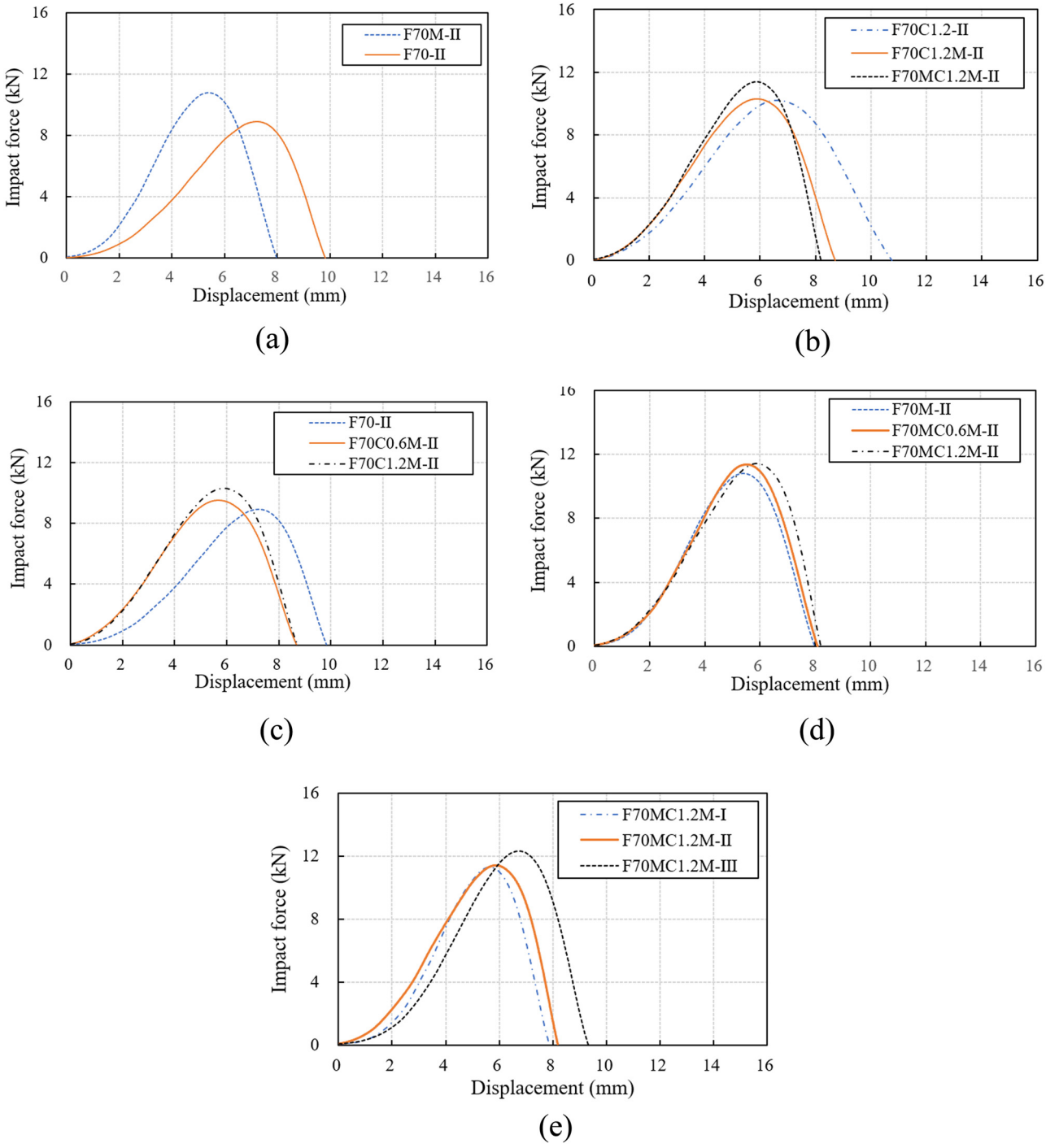


**Figure 9:** Impact force–displacement curves: (a) influence of the modified HGMs, (b) influence of the modified HGMs and MWCNTs, (c) influence of the contents of modified MWCNTs on specimens with unmodified HGMs, (d) influence of the contents of modified MWCNTs on specimens with modified HGMs, and (e) influence of the applied impact energy.

where the axial average stress $\bar{\sigma}_{cz}$ was calculated by averaging the FEA results.

$$\bar{\sigma}_{cz} = \frac{1}{A}\int_{A} \sigma_{cz}\left(x, y, \frac{L}{2}\right)\mathrm{d}x\mathrm{d}y, \tag{6}$$

$$G_{cxy} = \frac{TL}{\alpha J}, \tag{7}$$

$$J = \frac{8}{3}a^4, \tag{8}$$

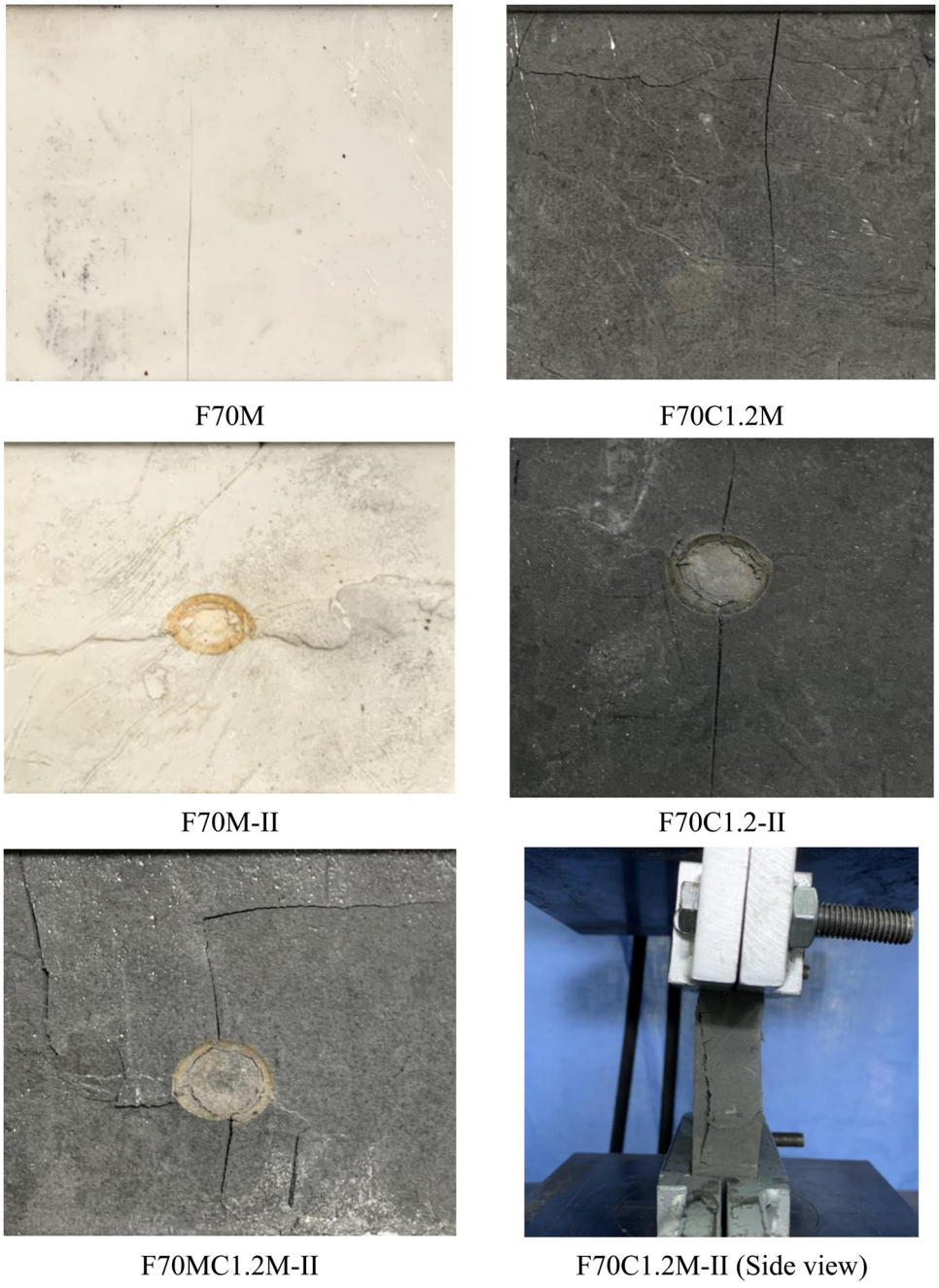


**Figure 10:** Edgewise compressive failure modes.

where $L$ and $2a$ are the lengths of RVEs in the $z$- and $y$-directions, respectively, $\Delta L$ and $\Delta a$ the deformations due to uniaxial compression and lateral contraction of RVEs, respectively, $A$ the cross-sectional area of RVEs, $T$ the applied torque on RVEs, $\alpha$ the rotational angle at the left end of RVEs, $J$ the average polar moments of inertia for the rectangular cross section, and $\Delta x$ the contraction in the $x$-direction due to the lateral pressure $p$.

To evaluate the effective mechanical properties of CNT-reinforced epoxy matrices, RVEs containing a long or a short CNT were modeled, and stresses and deformations of RVEs were computed for different load conditions to obtain the equivalent Young's moduli and Poisson's ratios of RVEs using equations (2)–(8). Abaqus/CAE 2019 was applied to model RVEs, in which, the 10-noded quadratic tetrahedron continuum element (C3D10) was used to

**Table 3:** Summary of edgewise compressive testing results

| Specimens | Strength of undamaged specimens (MPa) | CAI strength (MPa) | Strength retention factor |
|---|---|---|---|
| F70-II | 12.03 | 10.27 | 0.85 |
| F70C0.6-II | 13.95 | 12.27 | 0.88 |
| F70C1.2-II | 14.85 | 13.30 | 0.90 |
| F70M-I | 19.34 | 18.34 | 0.95 |
| F70M-II | | 18.02 | 0.93 |
| F70M-III | | 17.50 | 0.90 |
| F70C0.6M-I | 15.39 | 14.03 | 0.91 |
| F70C0.6M-II | | 13.50 | 0.88 |
| F70C0.6M-III | | 12.88 | 0.84 |
| F70C1.2M-I | 18.59 | 17.29 | 0.93 |
| F70C1.2M-II | | 17.12 | 0.92 |
| F70C1.2M-III | | 16.41 | 0.88 |
| F70MC0.6M-I | 21.63 | 20.81 | 0.96 |
| F70MC0.6M-II | | 20.42 | 0.94 |
| F70MC0.6M-III | | 19.97 | 0.92 |
| F70MC1.2M-I | 22.54 | 21.90 | 0.97 |
| F70MC1.2M-II | | 21.59 | 0.96 |
| F70MC1.2M-III | | 21.34 | 0.95 |

model the epoxy matrix and the triangular 3-noded shell element (S3) was used to model the CNT. The mesh sizes of the epoxy matrix and CNT were taken as 8.4 and 2.1 nm, respectively, because the further decreased element size almost generated the same results while the computational time increased significantly. The mechanical properties for long and short CNT RVEs extracted from the FE model are listed in Tables 4 and 5.

## 4.2 Unit cells of CNT-epoxy composites

A 3-D microscale unit cell was used to predict the effective mechanical properties in CNT-epoxy composites. The model was discretized into cubic elements. The averaged mechanical properties of the RVEs containing a single CNT were input into each element. Considering the average CNT length (15–30 μm), RVE size (130–300 nm), and CNT length distribution, the percentage of the elements represented by short CNT RVEs was taken as 20% [42]. The mechanical properties of the rest of the elements were represented by long CNT RVEs. CNT elements and the CNT orientation in each element were randomly generated using the Monte Carlo method (Figure 12 [47,48]). The uniaxial compressive test was conducted on the unit cell in the FE model to obtain the effective mechanical properties of the unit cell (Young's modulus $E_c$ and Poisson's $v_c$). The extracted mechanical property results of the CNT-epoxy composite unit cells are listed in Table 6.

## 4.3 Mechanical properties for RVEs of HGMs embedded in the CNT-epoxy matrix

This study further developed the use of simulation software Digimat 2017 to obtain the elastic modulus and Poisson's ratio of syntactic foam samples reinforced by CNTs. Digimat-MF is a material modeling and multiscale structural analytical software, in which a Mori-Tanaka mean-field homogenization scheme is applied to assess the behavior of composites [49–51]. RVE modeling of these samples is shown in Figure 13. The macroscopic behavior of samples was analyzed from the mechanical properties of unit cells of CNT-epoxy composites, with the CNT-epoxy matrix assumed to be elastic and particles assumed to be isotropic.

Uniaxial compressive testing was performed on the Digimat-MF platform to evaluate the elastic modulus and Poisson's ratio of samples reinforced with CNTs. For all foam composites analyzed, the particulars, such as weight fraction, particle shape (circle), size (mean diameter of 55 μm), particle distribution (diameter from 25 to 95 μm), and aspect ratio were defined at the macro level for inclusions. The aspect ratio was taken as 1/1 to confirm the generation of spherical inclusions [52].

The numerical results of the syntactic foam samples reinforced by MWCNTs are listed in Table 7. Comparisons between the numerical and measured elastic modulus of samples showed good agreement.

## 4.4 Modelling of syntactic foam under impact

The foam panel samples were assumed to be elastic and homogeneous with uniformly thin thickness [53]. The present specimens were modeled using Abaqus/CAE 2019, in which the elastic modulus and Poisson's ratio of syntactic foams were from Table 7. The steel impactor was simulated by an analytical rigid material that need not be meshed. The four sides of the samples were assumed to be fixed. C3D8R (eight-node linear brick reduced-integration hourglass control element) was used to model the syntactic foam samples, with a mesh size of 5 mm. Further decreasing the element size almost generated the same results while

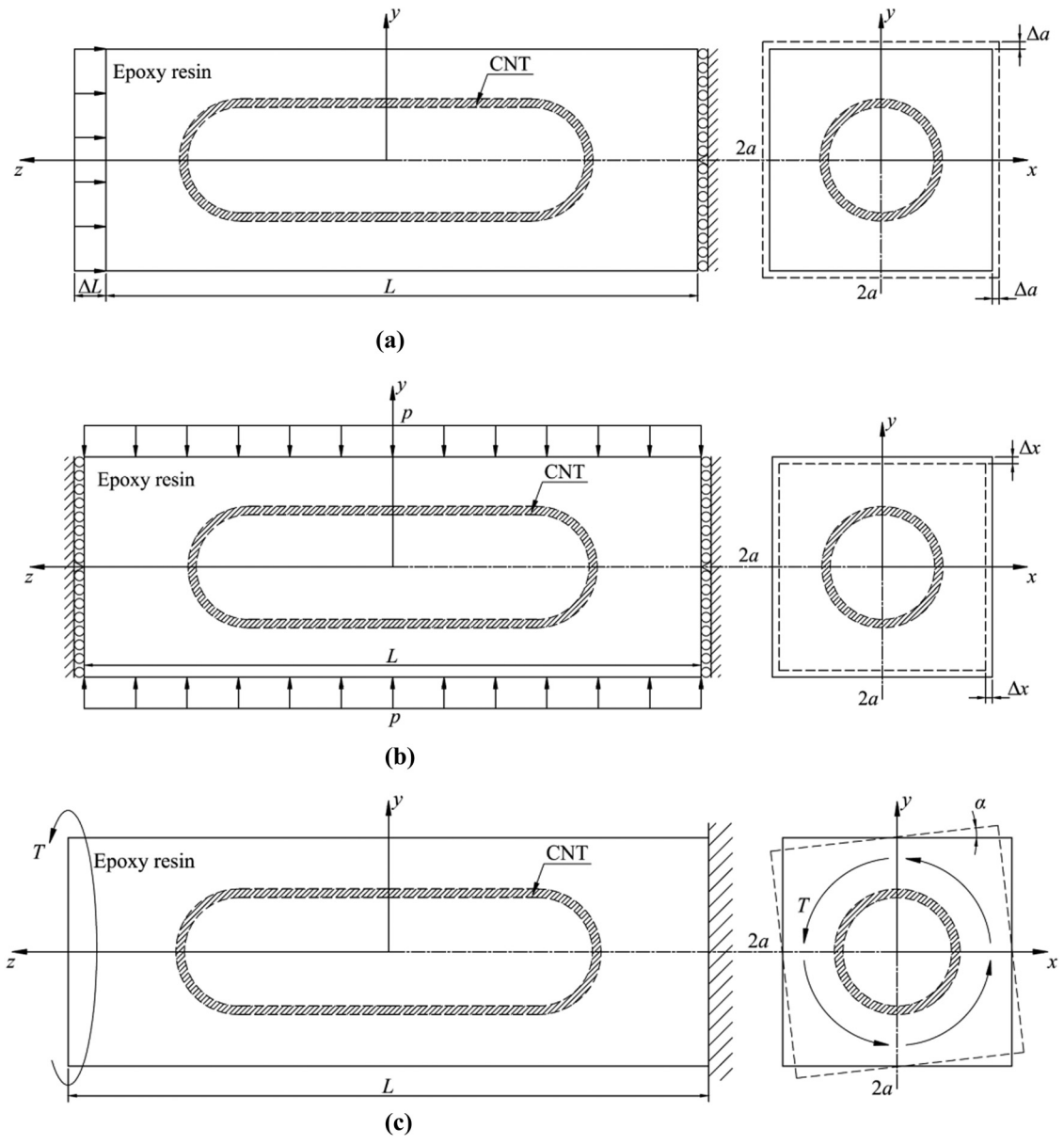


**Figure 11:** RVE containing a single CNT under different load conditions (left: front view and right: side view): (a) uniaxial compression, (b) lateral contraction, and (c) axial torsion.

**Table 4:** Material properties of long CNT RVEs extracted from the FE model

| Specimens | CNT (wt%) | CNT (vol%) | $E_{cz}$ (MPa) | $E_{cx} = E_{cy}$ (MPa) | $G_{cxy}$ (MPa) | $v_{czx} = v_{czy}$ | $v_{cxy}$ | $v_{cxz} = v_{cyz}$ ($=v_{czx}E_{cx}/E_{cz}$) |
|---|---|---|---|---|---|---|---|---|
| F70C0.6 | 0.6 | 0.15 | 879.34 | 482.56 | 164.95 | 0.329 | 0.463 | 0.181 |
| F70C1.2 | 1.2 | 0.31 | 1326.78 | 485.75 | 164.99 | 0.328 | 0.472 | 0.120 |
| F70C0.6M | 0.6 | 0.16 | 906.32 | 482.46 | 164.92 | 0.330 | 0.463 | 0.176 |
| F70C1.2M | 1.2 | 0.33 | 1380.07 | 485.89 | 165.04 | 0.329 | 0.472 | 0.116 |
| F70MC0.6M | 0.6 | 0.14 | 826.24 | 482.56 | 164.93 | 0.327 | 0.463 | 0.191 |
| F70MC1.2M | 1.2 | 0.27 | 1220.99 | 485.76 | 165.01 | 0.326 | 0.472 | 0.130 |

**Table 5:** Material properties of short CNT RVEs extracted from FE model

| Specimens | CNT (wt%) | CNT (vol%) | $E_{cz}$ (MPa) | $E_{cx} = E_{cy}$ (MPa) | $G_{cxy}$ (MPa) | $v_{czx} = v_{czy}$ | $v_{cxy}$ | $v_{cxz} = v_{cyz}$ ($=v_{czx}E_{cx}/E_{cz}$) |
|---|---|---|---|---|---|---|---|---|
| F70 | 0 | 0 | 435.00 | 435.00 | 163.53 | 0.330 | 0.330 | 0.330 |
| F70C0.6 | 0.6 | 0.15 | 473.19 | 442.72 | 165.61 | 0.329 | 0.337 | 0.308 |
| F70C1.2 | 1.2 | 0.31 | 505.73 | 445.64 | 165.65 | 0.328 | 0.345 | 0.289 |
| F70C0.6M | 0.6 | 0.16 | 475.29 | 442.62 | 165.58 | 0.330 | 0.337 | 0.307 |
| F70C1.2M | 1.2 | 0.33 | 509.34 | 445.77 | 165.70 | 0.328 | 0.345 | 0.287 |
| F70M | 0 | 0 | 435.00 | 435.00 | 163.53 | 0.330 | 0.330 | 0.330 |
| F70MC0.6M | 0.6 | 0.14 | 469.12 | 442.72 | 165.59 | 0.327 | 0.337 | 0.309 |
| F70MC1.2M | 1.2 | 0.27 | 498.42 | 445.65 | 165.67 | 0.326 | 0.345 | 0.291 |

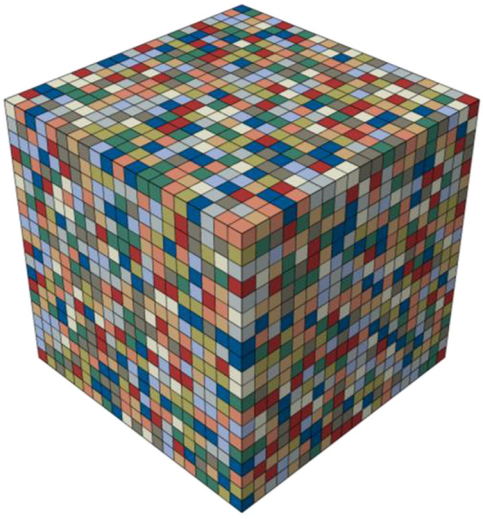

**Figure 12:** Random CNT orientation represented by different colors in a unit cell.

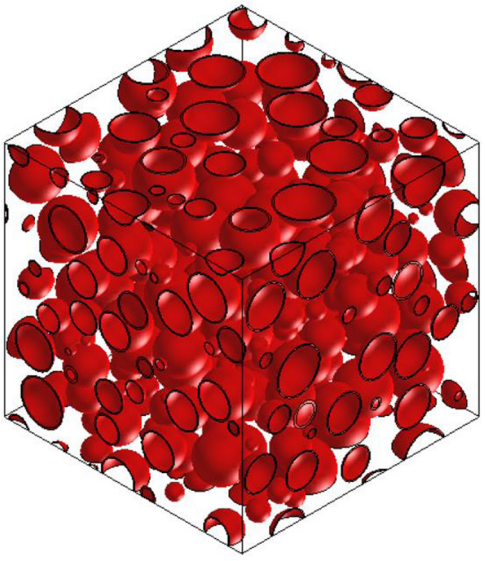

**Figure 13:** RVE modeling of syntactic foams.

**Table 6:** Young's modulus $E_c$ and Poisson's ratio $v_c$ for CNT-epoxy composite unit cells

| Specimens | CNT (wt%) | CNT (vol%) | $E_c$ (MPa) | $v_c$ |
|---|---|---|---|---|
| F70 | 0 | 0 | 435.00 | 0.330 |
| F70C0.6 | 0.6 | 0.15 | 636.35 | 0.324 |
| F70C1.2 | 1.2 | 0.31 | 820.15 | 0.310 |
| F70C0.6M | 0.6 | 0.16 | 647.30 | 0.323 |
| F70C1.2M | 1.2 | 0.33 | 841.89 | 0.309 |
| F70M | 0 | 0 | 435.00 | 0.330 |
| F70MC0.6M | 0.6 | 0.14 | 614.70 | 0.327 |
| F70MC1.2M | 1.2 | 0.27 | 777.11 | 0.312 |

**Table 7:** Comparisons of the mechanical properties of syntactic foams between the numerical and experimental results

| Specimens | $E_f$ (MPa) | $E_f'$ (MPa) | $\Delta = \frac{E_f' - E_f}{E_f} \times 100\%$ | $v$ |
|---|---|---|---|---|
| F70 | 600 | 617.70 | 2.95 | 0.251 |
| F70C0.6 | 630 | 671.92 | 6.65 | 0.249 |
| F70C1.2 | 710 | 718.14 | 1.15 | 0.248 |
| F70C0.6M | 680 | 693.92 | 2.05 | 0.249 |
| F70C1.2M | 780 | 743.63 | −4.66 | 0.248 |
| F70M | 730 | 730.80 | 0.11 | 0.251 |
| F70MC0.6M | 970 | 900.70 | −7.14 | 0.249 |
| F70MC1.2M | 1,060 | 956.97 | −9.72 | 0.248 |

the computational time was remarkably prolonged. Specimens were impacted by the steel impactor with certain initial velocities and the surface-to-surface contact elements were applied to simulate the interface between the impactor and sample.

Stress contours of a typical sample (F70MC0.6M-I) under impact are shown in Figure 14. The Mises stress

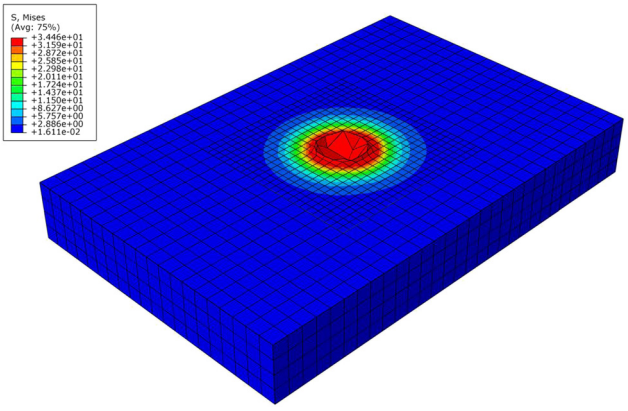


**Figure 14:** Stress contour of specimen F70MC0.6M-I.

reached high levels at the sample center and gradually decreased toward the edges, resulting in a dent in the sample center. The numerical impact responses were in good agreement with the experimental results (Table 8 and Figure 15).

## 4.5 Parametric studies

The verified FE model was used to analyze the influence of CNT types and diameter-to-thickness ratios of HGMs on the impact responses of these samples. The impact responses of samples reinforced by MWCNTs were compared with those of samples reinforced by helical MWCNTs (HMWCNTs; Figure 16a and b). These HMWCNTs had outer diameters of 100–200 nm, length of 1–10 μm, bulk density of 0.483 g/cm$^3$, Young's modulus of 1,054 GPa, and Poisson's ratio of 0.25; these properties were provided by Chengdu Jiacai Technology Co., Ltd., China. In cases of the same CNT content and the same applied impact energy, the peak-impact force, and duration of specimens reinforced by HMWCNTs were a little higher than those of specimens reinforced by MWCNTs (*i.e.*, F70MC0.6M-I and F70MC1.2M-I, respectively), resulting in ~14% increase of SEA in the former.

Three different diameter-to-thickness ratios (*i.e.*, 48, 58, and 68) of HGMs were applied in specimen F70 MC1.2M-I. Increasing the diameter-to-thickness ratio of HGMs from 48 to 68 was found to result in a 19% decrease

**Table 8:** Comparisons of the peak-impact forces and duration of syntactic foam panels between the numerical and experimental results

| Specimens | $F_{max}$ (kN) | $F'_{max}$ (kN) | $\Delta = \frac{F'_{max} - F_{max}}{F_{max}} \times 100\%$ | $T$ (ms) | $T'$ (ms) | $\Delta = \frac{T' - T}{T} \times 100\%$ |
|---|---|---|---|---|---|---|
| F70-I | 8.19 | 8.01 | −2.17 | 3.03 | 3.08 | 1.73 |
| F70C0.6-I | 8.83 | 8.92 | 0.97 | 3.14 | 3.13 | −0.18 |
| F70C1.2-I | 9.57 | 9.10 | −4.90 | 3.36 | 3.19 | −5.05 |
| F70C0.6M-I | 9.10 | 9.21 | 1.20 | 2.98 | 2.92 | −2.29 |
| F70C1.2M-I | 9.62 | 9.74 | 1.23 | 3.01 | 2.91 | −3.32 |
| F70M-I | 10.04 | 10.14 | 1.03 | 2.56 | 2.47 | −3.44 |
| F70MC0.6M-I | 11.02 | 11.00 | −0.19 | 2.82 | 2.85 | 1.06 |
| F70MC1.2M-I | 11.28 | 11.56 | 2.46 | 2.90 | 2.86 | −1.56 |
| F70-II | 8.92 | 8.60 | −3.59 | 3.23 | 3.38 | 4.51 |
| F70C0.6-II | 9.46 | 9.30 | −1.72 | 3.38 | 3.54 | 4.86 |
| F70C1.2-II | 10.21 | 10.33 | 1.20 | 3.54 | 3.34 | −5.62 |
| F70C0.6M-II | 9.51 | 9.74 | 2.37 | 3.20 | 3.09 | −3.55 |
| F70C1.2M-II | 10.30 | 10.25 | −0.52 | 3.31 | 3.21 | −2.95 |
| F70M-II | 10.80 | 11.05 | 2.29 | 2.72 | 2.71 | −0.51 |
| F70MC0.6M-II | 11.36 | 11.38 | 0.19 | 2.85 | 2.94 | 3.28 |
| F70MC1.2M-II | 11.50 | 11.25 | −2.17 | 2.92 | 2.88 | −1.44 |
| F70C0.6M-III | 9.90 | 10.04 | 1.46 | 3.43 | 3.30 | −3.93 |
| F70C1.2M-III | 10.49 | 10.71 | 2.06 | 3.69 | 3.46 | −6.18 |
| F70M-III | 11.43 | 11.57 | 1.25 | 2.89 | 2.90 | 0.35 |
| F70MC0.6M-III | 12.05 | 11.99 | −0.47 | 3.02 | 2.92 | −3.39 |
| F70MC1.2M-III | 12.31 | 12.04 | −2.16 | 3.11 | 3.12 | 0.27 |

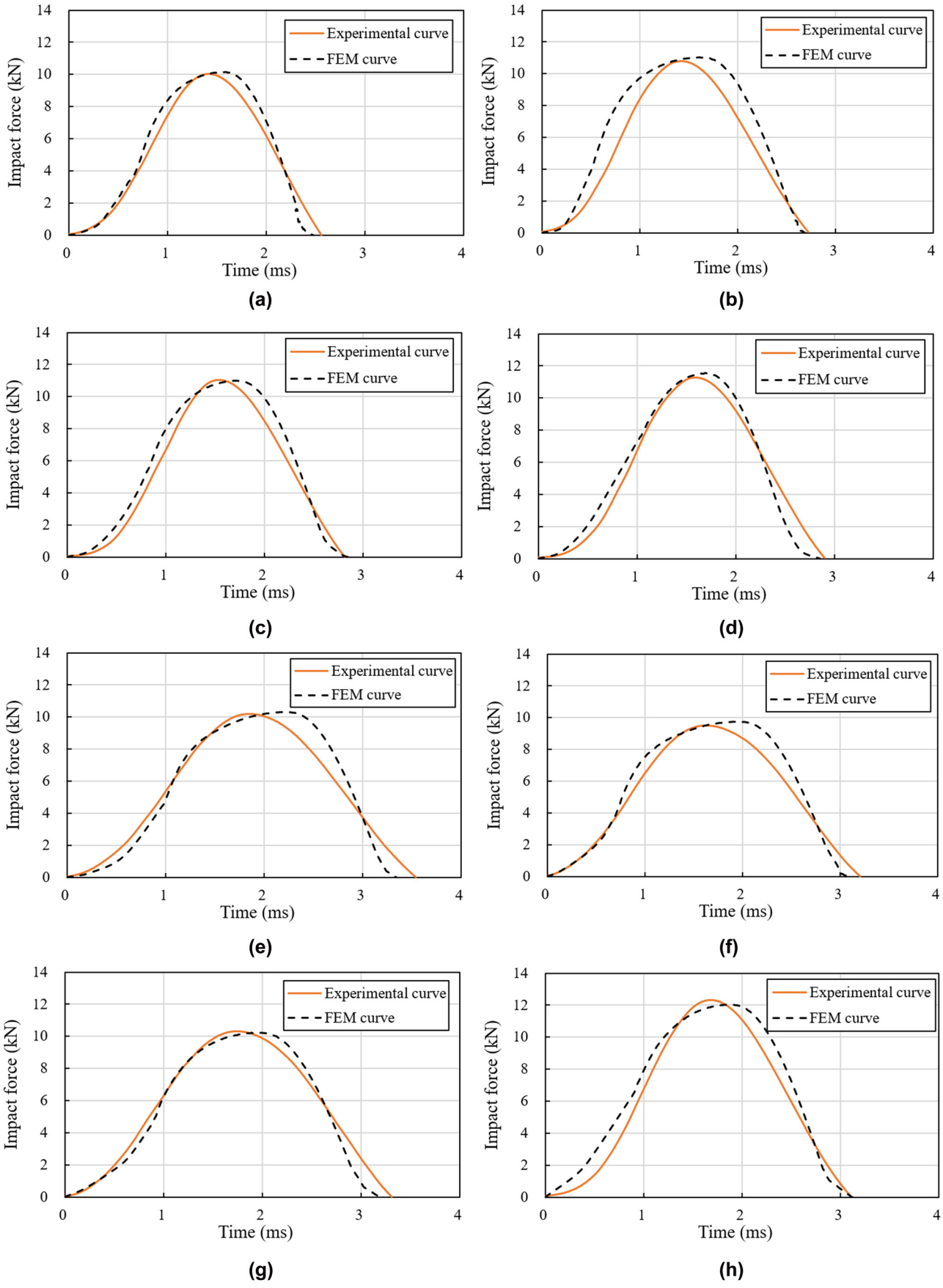


**Figure 15:** Comparison of numerical and experimental impact force histories for typical specimens: (a) F70M-I, (b) F70M-II, (c) F70MC0.6M-I, (d) F70MC1.2M-I, (e) F70C1.2-II, (f) F70C0.6M-II, (g) F70C1.2M-II, and (h) F70MC1.2M-III.

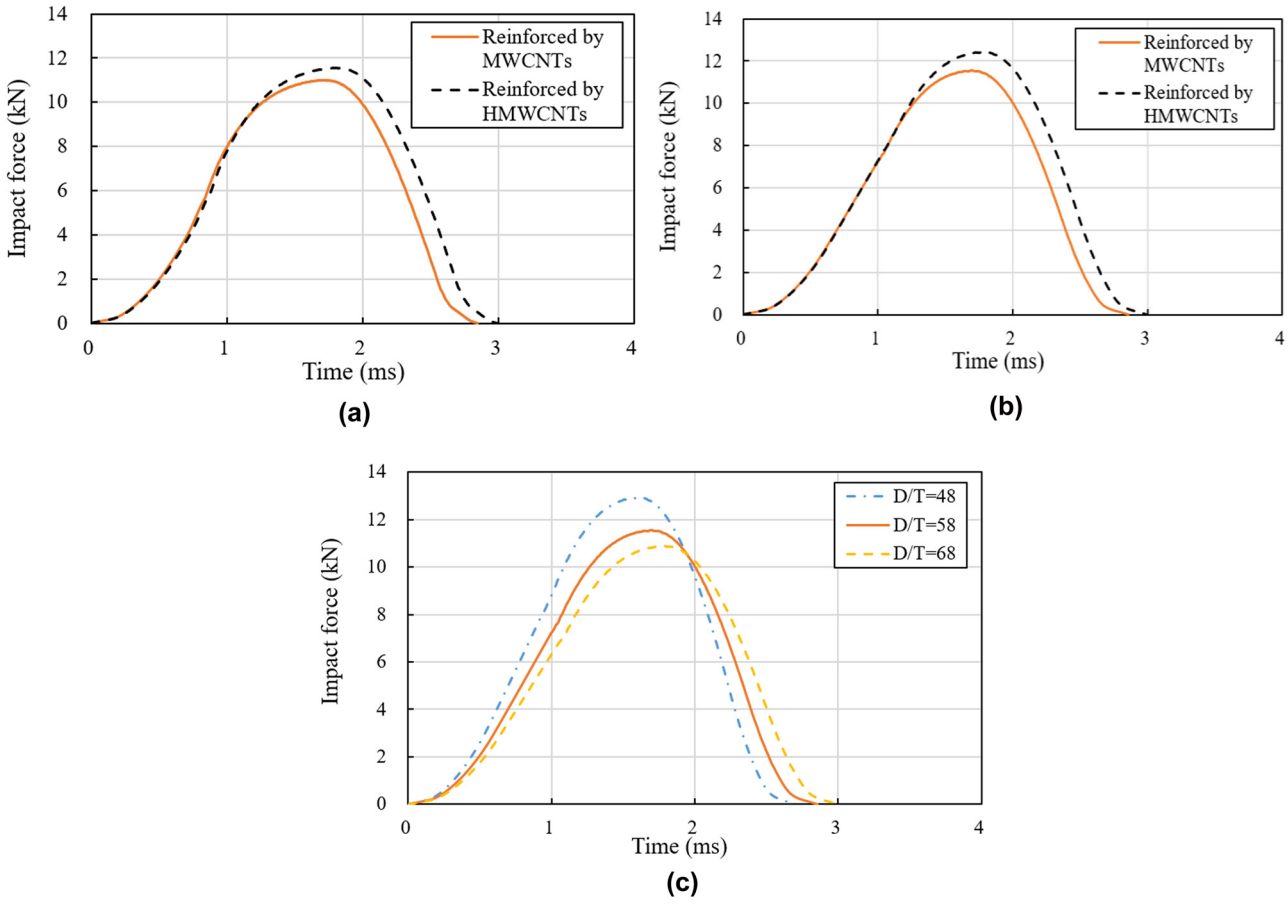


**Figure 16:** Parametric studies by verified FE model: (a) F70MC0.6M-I reinforced by different CNT types, (b) F70MC1.2M-I reinforced by different CNT types, and (c) F70MC1.2M-I with different diameter-to-thickness ratios (D/T).

in the peak-impact force and 10% increase in duration, as well as a 5% decrease in SEA (Figure 16c).

## 5 Conclusion

The impact responses of modified HGMs and MWCNTs incorporated in the epoxy resin matrix syntactic foam panel samples were investigated. The results were as follows:

(1) The MPD of specimens with modified HGMs and MWCNTs were smaller than those of specimens with unmodified HGMs and MWCNTs, which indicated that modified HGMs and MWCNTs led to increased local stiffness of these syntactic foams.

(2) Modifying HGMs by amine treatment was an effective means for enhancing the impact resistance and energy absorption ability of these composites, while merely modifying MWCNTs by acid treatment had an insignificant influence on the composite impact resistance and energy absorption ability.

(3) Modifying both HGMs and MWCNTs contributed to an increased CAI strength of panel samples, with CAI strength increased with increased modified MWCNT contents because modifying HGMs enhanced the interfacial adhesion between filler-resin interfaces and crack propagation was hindered by MWCNTs.

(4) Multiscale FE models were developed to simulate the impact behavior of syntactic foam samples. RVEs containing a single CNT were modeled to extract the equivalent mechanical properties of nano-hetero-structures. Then, a 3-D microscale unit cell was modeled to obtain the compressive properties of CNT-epoxy composites, which were then input in RVE modeling of these samples. The impact responses of samples were then analyzed in ABAQUS and the numerical results were found to agree well with the test data.

(5) The verified FE model was then used to analyze the influence of CNT type and the diameter-to-thickness

ratio of HGMs. Numerical results indicated that, in the case of constant CNT content, samples reinforced by HMWCNTs had a little higher impact resistance and energy absorption ability than the panels reinforced by MWCNTs. A larger diameter-to-thickness ratio of HGMs resulted in a lower peak-impact force and energy absorption ability, as well as longer duration in these samples.

(6) The syntactic foam composites incorporated with amine-treated HGMs and acid-treated MWCNTs exhibited lightweight, high impact resistance, and high-energy absorption ability, which can be applied as load-carrying members or energy dissipative elements. However, merely modified MWCNTs have an insignificant influence on the enhancement of impact resistance and energy absorption ability. Further research may be needed to focus on investigating the effects of other functionalization treatments of MWCNTs and the alignment of MWCNTs.

**Funding information:** This study was financially supported by the National Natural Science Foundation of China (Grant 51578283), Top Six Talent Projects in Jiangsu Province, China (Grant No. JZ-024), Science and Technology projects in Jiangsu Construction System, China (Grant 2021ZD05), and Postgraduate Research and Practice Innovation Program of Jiangsu Province, China (Grant No. KYCX21_1154).

**Author contributions:** Yi Wang: Numerical analysis, validation, writing – original draft. Jun Wang: Investigation, conceptualization, formal analysis, resources, project administration, writing – review and editing. Jie Wang: Formal analysis, validation, experimental study. David Hui: Visualization. All authors have accepted responsibility for the entire content of this manuscript and approved its submission.

**Conflict of interest:** David Hui, who is the co-author of this article, is a current Editorial Board member of *Nanotechnology Reviews*. This fact did not affect the peer-review process. The authors declare no other conflict of interest.

# References

[1] Wu X, Gao Y, Wang Y, Fan R, Ali Z, Yu J, et al. Recent developments on epoxy-based syntactic foams for deep sea exploration. J Mater Sci. 2021;56(3):2037–76.

[2] Wang J, Li J, GangaRao H, Liang R, Chen J. Low-velocity impact responses and CAI properties of synthetic foam sandwiches. Compos Struct. 2019;220:412–22.

[3] Lu Z, Li J, Xie J, Huang P, Xue L. Durability of flexurally strengthened RC beams with prestressed CFRP sheet under wet–dry cycling in a chloride-containing environment. Compos Struct. 2021;255:112869.

[4] Ding J, Liu Q, Ye F, Zhang H, Gao Y, Zhang B. Compressive properties of co-continuous hollow glass microsphere epoxy resin syntactic foams prepared using resin transfer molding. J Reinf Plast Comp. 2020;39(3–4):132–43.

[5] Qi C, Yu Q, Zhao Y. Fabrication and characterization of the thermoplastic and thermoset syntactic foam core-based sandwich composites. Polym Composite. 2020;41(8):3052–61.

[6] Kaur M, Jayakumari LS. Consequence of cenosphere loading on hygrothermal, thermal, and mechanical properties of epoxy syntactic foams. J Cell Plast. 2019;55(3):297–318.

[7] Breunig P, Damodaran V, Shahapurkar K, Wadder S, Doddamani M, Jeyaraj P, et al. Dynamic impact behavior of syntactic foam core sandwich composites. J Compos Mater. 2020;54(4):535–47.

[8] Ullas AV, Sharma PK, Chandel P, Sharma P, Kumar D, Roy PK, et al. Epoxy-glass microballoon syntactic foams for blast mitigating applications. Defence Sci J. 2018;68(2):210–7.

[9] Rostilov TA, Ziborov VS. Experimental study of shock wave structure in syntactic foams under high-velocity impact. Acta Astronaut. 2021;178:900–7.

[10] Yousaf Z, Smith M, Potluri P, Parnell W. Compression properties of polymeric syntactic foam composites under cyclic loading. Compos Part B-Eng. 2020;186:107764.

[11] Domun N, Hadavinia H, Zhang T, Sainsbury T, Liaghat GH, Vahid S. Improving the fracture toughness and the strength of epoxy using nanomaterials-a review of the current status. Nanoscale. 2015;7:10294–329.

[12] Zengin H, Siddiqui JA, Ottenbrite RM. Glass bead grafting with poly (carboxylic acid) polymers and maleic anhydride copolymers. Polym Advan Technol. 2008;19(2):105–13.

[13] Zhang L, Zhang J, Wang DY. Hierarchical layered double hydroxide nanosheets/phosphorus-containing organosilane functionalized hollow glass microsphere towards high performance epoxy composite: Enhanced interfacial adhesion and bottom-up charring behavior. Polymer. 2020;210:123018.

[14] Imran M, Rahaman A, Pal S. Effect of low concentration hollow glass microspheres on mechanical and thermomechanical properties of epoxy composites. Polym Composite. 2019;40(9):3493–9.

[15] Mutua FN, Lin P, Koech JK. Surface modification of hollow glass microspheres. Mater Sci Appl. 2012;3(12):856–60.

[16] Hu Y, Yu Z, Fan G, Tan Z, Zhou J, Zhang H, et al. Simultaneous enhancement of strength and ductility with nano dispersoids in nano and ultrafine grain metals: a brief review. Rev Adv Mater Sci. 2020;59(1):352–60.

[17] Mishra SK. Toughening of nanocomposite hard coatings. Rev Adv Mater Sci. 2020;59(1):553–85.

[18] Song Z, Li Y, Yang B. The interfacial load-transfer enhancement mechanism of amino-functionalised carbon nanotube reinforced epoxy matrix composites: a molecular dynamics study. Compos Sci Technol. 2021;209:108790.

[19] Duan K, Li L, Wang F, Liu S, Hu Y, Wang X. New insights into interface interactions of CNT-reinforced epoxy nanocomposites. Compos Sci Technol. 2021;204:108638.
[20] Esmaeili A, Ma D, Manes A, Oggioni T, Jimenez-Suarez A, Urena A, et al. An experimental and numerical investigation of highly strong and tough epoxy based nanocomposite by addition of MWCNTs: Tensile and mode I fracture tests. Compos Struct. 2020;252:112692.
[21] Wang B, Bai Y, Hu X, Lu P. Enhanced epoxy adhesion between steel plates by surface treatment and CNT/short-fibre reinforcement. Compos Sci Technol. 2016;127:149–57.
[22] Laurenzi S, Pastore R, Giannini G, Marchetti M. Experimental study of impact resistance in multi-walled carbon nanotube reinforced epoxy. Compos Struct. 2013;99:62–8.
[23] Wu Q, Miao W, Zhang Y, Gao H, Hui D. Mechanical properties of nanomaterials: a review. Nanotechnol Rev. 2020;9(1):259–73.
[24] Yang H, Yang Y, Liu Y, He D, Bai J. Multi-scale study of CNT and CNT-COOH reinforced epoxy composites: dispersion state, interfacial interaction vs mechanical properties. Compos Interface. 2021;28(4):381–93.
[25] Jian W, Lau D. Understanding the effect of functionalization in CNT-epoxy nanocomposite from molecular level. Compos Sci Technol. 2020;191:108076.
[26] Kocaman S, Gursoy M, Karaman M, Ahmetli G. Synthesis and plasma surface functionalization of carbon nanotubes for using in advanced epoxy-based nanocomposites. Surf Coat Tech. 2020;399:126144.
[27] Li S, Wang F, Wang Y, Wang J, Ma J, Xiao J. Effect of acid and TETA modification on mechanical properties of MWCNTs/epoxy composites. J Mater Sci. 2008;43(8):2653–8.
[28] Guzman ME, Rodriguez AJ, Minaie B, Violette M. Processing and properties of syntactic foams reinforced with carbon nanotubes. J Appl Polym Sci. 2012;124(3):2383–94.
[29] Ya B, Wang Y, Meng L, Zhou B, Zhang X. Study on the performance of syntactic foam reinforced by hybrid functionalized carbon nanotubes. J Appl Polym Sci. 2020;137(16):48586.
[30] Ciecierska E, Boczkowska A, Kurzydlowski KJ, Rosca ID, Van, Hoa S. The effect of carbon nanotubes on epoxy matrix nanocomposites. J Therm Anal Calorim. 2013;111(2):1019–24.
[31] Ghosh D, Wiest A, Conner RD. Uniaxial quasistatic and dynamic compressive response of foams made from hollow glass microspheres. J Eur Ceram Soc. 2016;36(3):781–9.
[32] Phama TM, Chen W, Kingston J, Hao H. Impact response and energy absorption of single phase syntactic foam. Compos Part B-Eng. 2018;150:226–33.
[33] Ahmadi H, Liaghat G, Charandabi SC. High velocity impact on composite sandwich panels with nano-reinforced syntactic foam core. Thin Wall Struct. 2020;148:106599.
[34] Siegfried M, Tola C, Claes M, Lomov SV, Verpoest I, Gorbatikh L. Impact and residual after impact properties of carbon fiber/epoxy composites modified with carbon nanotubes. Compos Struct. 2014;111:488–96.
[35] Bao F, Wang J, Wang J, Zeng S, Guo X. Static and impact responses of syntactic foam composites reinforced by multi-walled carbon nanotubes. J Mater Res Technol. 2020;9(6):12391–403.
[36] ASTM D1621-10. Standard test method for compressive properties of rigid cellular plastics. PA, USA; 2010.
[37] ASTM D638-02a. Standard test method for tensile properties of plastics. PA, USA; 2002.
[38] ASTM D7136M-15. Standard test method for measuring the damage resistance of a fiber-reinforced polymer matrix composite to a drop-weight impact event. PA, USA; 2015.
[39] ASTM D7137/7137M-12. Standard test method for compressive residual strength properties of damaged polymer matrix composite plates. West Conshohocken, PA, USA; 2012.
[40] Liu X, Qian C, Yu K, Jiang Y, Fu Q, Qian K. Energy absorption and low-velocity impact response of shear thickening gel reinforced polyurethane foam. Smart Mater Struct. 2020;29(4):045018.
[41] Castro G, Nutt SR, Wenchen X. Compression and low-velocity impact behavior of aluminum syntactic foam. Mat Sci Eng A. 2013;578:222–9.
[42] Hu Z, Arefin MRH, Yan X, Fan QH. Mechanical property characterization of carbon nanotube modified polymeric nanocomposites by computer modeling. Compos Part B-Eng. 2014;56:100–8.
[43] Dastmard MH, Ansari R, Rouhi S. Prediction of axial Young's modulus of epoxy matrix reinforced by group-IV nanotube: a finite element investigation. Mech Mater. 2021;157:103819.
[44] Arora G, Pathak H. Experimental and numerical approach to study mechanical and fracture properties of high-density polyethylene carbon nanotubes composite. Mater Today Commun. 2020;22:10089.
[45] Timoshenko S, Goodier J. Theory of elasticity. New York: McGraw-Hill; 1987.
[46] Golestanian H, Shojaie M. Numerical characterization of CNT-based polymer composites considering interface effects. Comp Mater Sci. 2010;50(2):731–6.
[47] Ma D, Giglio M, Manes A. An investigation into mechanical properties of the nanocomposite with aligned CNT by means of electrical conductivity. Compos Sci Technol. 2020;188:107993.
[48] Chen X, Alian AR, Meguid SA. Modeling of CNT-reinforced nanocomposite with complex morphologies using modified embedded finite element technique. Compos Struct. 2019;227:111329.
[49] Hamidreza A, Mertiny PM. Composite polymer with random distribution of spherical particles. Canadian International Conference on Composite Materials; 2015.
[50] Banal M, Chatzigeorgiou G, Meraghni F, Leon R. Homogenization using modified Mori-Tanaka and TFA framework for elastoplastic-viscoelastic-viscoplastic composites: theory and numerical validation. Int J Plasticity. 2020;127:102632.
[51] Trzepiecinski T, Ryzinska G, Biglar M, Gromada M. Modelling of multilayer actuator layers by homogenisation technique using Digimat software. Ceram Int. 2017;43(3):3259–66.
[52] Das Lala S, Sadikbasha S, Deoghare AB. Prediction of elastic modulus of polymer composites using Hashin–Shtrikman bound, mean field homogenization and finite element technique. P I Mech Eng C-J Mec. 2020;234(8):1653–9.
[53] Wang JF, Yang JP, Tam LH, Zhang W. Molecular dynamics-based multiscale nonlinear vibrations of PMMA/CNT composite plates. Mech Syst Signal Pr. 2021;153:107530.